Aluminum Local Environment and Defects in the Crystalline Structure of Sol−Gel Alumina Catalyst

J. A. Wang, X. Bokhimi, A. Morales, and O. Novaro†

Institute of Physics, The National University of Mexico (UNAM), A. P. 20-364, 01000 México D. F., Mexico

T. López and R. Gómez*

Department of Chemistry, Universidad Autónoma Metropolitana-I, A. P. 55-534, 09340 México D.F., Mexico

Received: July 23, 1998; In Final Form: October 5, 1998

Nanocrystalline alumina was synthesized by using the sol−gel method with aluminum *sec*-butoxide as the precursor. FTIR, TG, XRD, and crystalline structure refinement were used to analyze the phase transformations and their crystalline structures. When samples were annealed at 200 °C, they had two nanocrystalline phases γ-boehmite and γ*-boehmite, which had the same crystalline structure but different lattice parameters and defect numbers in the structure. After sample annealing above 400 °C, the γ-boehmite and γ*-boehmite phases were transformed into nanocrystalline γ-Al_2O_3 and θ-Al_2O_3. The γ-alumina crystalline structure contained hydroxyls that brought about cationic defects in aluminum sites, mainly in those of octahedral symmetry. In the ^{27}Al NMR spectra of the samples calcined at 400, 600, and 800 °C, a chemical shift around 33 ppm was observed, which occurred between that of aluminum in oxygen octahedra and aluminum in oxygen tetrahedra. Its origin can be explained by assuming the existence the substitution of some lattice oxygen ions in the octahedral symmetry by hydroxyl groups.

Introduction

Because of their high specific surface areas and the large number of defects in their crystalline structure, the low-temperature alumina phases are important in catalysis.[1−8] Their small crystallite sizes, however, were difficult to characterize. Nevertheless, the recent important interest in nanocrystalline materials has helped to develop characterization techniques for samples made of small crystallite sizes.

Of these techniques, some of them are common in many laboratories, for example, nuclear magnetic resonance (NMR), which can observe the local order, and X-ray diffraction, from which, by refining the crystalline structures, lattice parameters, crystalline phase abundance, and vacancy concentrations can be estimated.[9−11] Therefore, it is possible to reanalyze systems that have phases with a very small crystallite size, as is the case of γ-alumina.

For the present work, we used the techniques mentioned above to identify the local environment of aluminum atoms and to estimate the relative abundance of aluminum and oxygen vacancies in the alumina lattice. The study was done in alumina prepared from the hydrolysis of aluminum alkoxides (sol−gel method) due to the facilities to obtain alumina showing important structural hydroxylation.

Seven crystalline phases have been reported for alumina: η, γ, χ, δ, κ, θ, and α.[12] From them, only α-alumina can be invariably obtained at thermal treatment above 1000 °C. The other alumina phases appear always mixed, because the transition temperature range between them is very sharp. Therefore, to obtain the crystalline structure parameters characterizing these phases is certainly an interesting undertaking.[9,13−16]

The transformation between alumina phases strongly depends on the precursors and the thermal treatment used in their stabilization. For instance, the thermal dehydration of trihydrates or gibbsite yields only boehmite (AlO(OH)), which by additional annealing is transformed into γ-Al_2O_3 .[15] This contrasts with diaspora, which, under hydrothermal treatment, dehydrates to form corundum.[17,18] Defects in the crystalline structure appear to be important, especially in the initial transformation stages.

Vacancies are the most frequent defects found in alumina. When they are at the crystal surface, basic and acid sites are generated,[19−25] determining its catalytic properties. A precise knowledge of the structural defect character (anionic and cationic) certainly will help in understanding their role in catalysis.

The small crystallite size of low-temperature alumina phases makes the study of the vacancies and their relative abundance more difficult. Recently, however, it has been shown that some of the vacancy properties in nanocrystalline materials can be inferred by refining the crystalline structure of the phases in the sample.[9−11] This is done by modeling the crystalline structure and size effects; the model is used for simulating the X-ray of the neutron diffraction pattern produced by the sample. The parameters involved in the model are varied until the theoretical diffraction pattern fits as well as possible to the experimental results. This technique, developed by H. Rietveld,[26] is used for refining crystalline structures by starting from polycrystalline samples. The refinement also provides information about phase concentrations, which, for nanocrystalline samples, are difficult to obtained with other techniques. In the present study, this technique was used for refining the crystalline structure of the phases in the samples.

The main interest of the present paper was to study the low-temperature phases of alumina. Because of their importance in

* To whom correspondence should be addressed. Phone: (525) 724 4668. Fax: (525) 724 4666. E-mail: gomr@xanum.uam.mx.

† Member of El Colegio Nacional, Mexico.

10.1021/jp983130r CCC: $18.00
Published on Web 12/19/1998

heterogeneous catalysis, in particular, we were interested in analyzing the type of vacancies in the crystalline structures and the local environments associated with the aluminum atoms.

Thermal dehydration of aluminum hydroxides, chemical vapor deposition, and the sol−gel technique are examples of the methods used to prepare alumina.[27−31] From them, we chose the sol−gel technique because it produces samples with a large specific surface area and provides a better control of synthesis conditions and sample purity. Phase transformations were analyzed with thermogravimetry and X-ray powder diffraction; the evolution of hydroxyl with temperature was measured with fourier infrared (FTIR) spectroscopy. Vacancy and phase concentrations were obtained from the refinement of the crystalline structures. Finally, the local environment of the aluminum atom was obtained from NMR spectroscopy and the refinement.

Experimental Section

Catalyst Synthesis. In buthanol, 25.73 mL of aluminum tri-*sec*-butoxide (Aldrich, 99%) was dissolved. To this solution, 1 g of oxalic acid (Baker, 99%), the hydrolysis catalyst, was added to obtain pH 5. Thereafter, 15 mL of water were slowly dropped into the solution, which was refluxed and stirred for 3 h at 70 °C until forming a gel. Before characterization, samples were dried at 70 °C and annealed in air at 200, 400, 600, and 800 °C for 8 h.

Catalyst Characterization. *Thermogravimetric Analysis (TGA).* Thermogravimetric analysis was carried out in a DuPont 2100 thermoanalyzer. The sample (20 mg), in a quartz pan, was heated in flowing air from room temperature to 800 °C at 10 °C/min.

FTIR Spectroscopy. Samples were characterized by FTIR spectroscopy with a 170-SX Nicolet spectrometer. Self-supported sample wafers were mounted in a glass cell with KBr windows. Spectra were recorded at different temperatures in a vacuum.

NMR Spectroscopy. Magic angle spinning NMR (MAS-NMR) spectra in ^{27}Al isotope were recorded with an ASX300 Bruker spectrometer at a spectral frequency of 300.13 MHz and a width of 50 000 Hz. Measurements were carried out at room temperature with a 10 μs pulse length (90°); $Al(H_2O)_6^{3+}$ was the chemical shift reference.

X-ray Diffraction and Rietveld Refinement. X-ray diffraction patterns were measured at room temperature with a Siemens D-5000 diffractometer having Cu $K\alpha$ radiation and a secondary-beam graphite monochromator. Intensities were measured in the 8−110° 2θ range with a 0.02° step size and a measuring time of 1.03 s per point. The DBWS-9600PC[32] and WYRIET[33] programs were used for refining the crystalline structures with the Rietveld method.

Results and Discussion

Weight Loss and Dehydroxylation. Three weight loss regions were observed in the TGA-DTG curve (Figure 1). The weight loss of 17.1 wt % between 20 and 170 °C was attributed to the desorption of physically adsorbed water and organic molecules. Desorption of chemisorbed water molecules and residual organic groups occurred between 170 and 248 °C and produced a weight loss of only 4.4 wt %. The pronounced weight loss of 15.3 wt %, observed between 248 and 513 °C, was produced by dehydroxylation of the sample during the transformation of γ-boehmite into alumina. According to this transformation (eq 1), a weight loss of 15 wt % should be achieved, which is very near to the one measured.

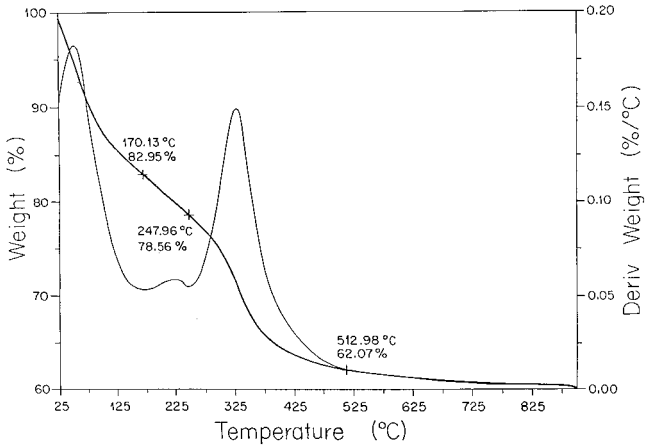

Figure 1. TGA-DTG profile of sol−gel alumina in air.

$$2AlO(OH) \rightarrow Al_2O_3 + H_2O \quad (1)$$

The extra 0.3 wt % weight loss could be produced by the further desorption of the adsorbed species. This result showed that boehmite decomposition was almost complete in this temperature range. Above 520 °C, although the sample did not have any weight loss step, the TGA curve continued descending; this is caused by the gradual loss of the hydroxyl groups in the crystalline structure.

Hydroxyl Evolution with Temperature. Hydroxyl stretching vibrations produced FTIR absorption bands between 2800 and 4000 cm^{-1} (Figure 2). The fresh sample, dried at 70 °C, had an intense and wide absorption band at 3455 cm^{-1} (Figure 2a), which resulted from the hydroxyls on the γ-AlO(OH) surface. When the annealing temperature increased from 70 to 400, 600, and 800 °C, the intensity of this band diminished, due to the desorption of adsorbed water molecules and boehmite decomposition, but it never disappeared. At 800 °C, hydroxyl bands were still observed, which reflects the high capacity of the alumina phases for retaining hydroxyls in their structures. This explains the slow decrease observed in the TG curve above 520 °C.

Crystalline Structures and Phase Transformations. Crystalline structures were refined by using the Rietveld technique. Tables 1−3 give the atom coordinates in the unit cell used for the refinement. Table 1 corresponds to γ-AlO(OH), which has an orthorhombic unit cell with space group *Cmcm*. Table 2 corresponds to γ-Al_2O_3, which has a cubic unit cell with space group *Fd*3*m*. Table 3 corresponds to θ-Al_2O_3, which has a monoclinic unit cell with space group *C*2/*m*. Diffraction peaks were broad and diffuse because the crystallites were very small and imperfect. All phases in the samples were nanocrystalline (Figure 3).

In the fresh samples, only boehmite was found; it has a crystalline structure built up of layers, made up of sharing corner octahedra, parallel to the (100) plane. The octahedra are nearly regular and have four of their corners occupied by oxygen atoms and the other two by hydroxyls. Oxygen atoms are close packed, but the structure as a whole is not close packed.[34]

The fresh-sample experimental diffraction pattern was not correctly modeled if the sample only contained γ-AlO(OH). The difference between the theoretical and experimental diffraction patterns was large. The difference was reduced when the diffraction pattern was modeled with a mixture of two crystalline phases. The second phase had the same crystalline structure as γ-AlO(OH); therefore, it was named γ*-boehmite. When samples were annealed at 400 °C, the following parameters were

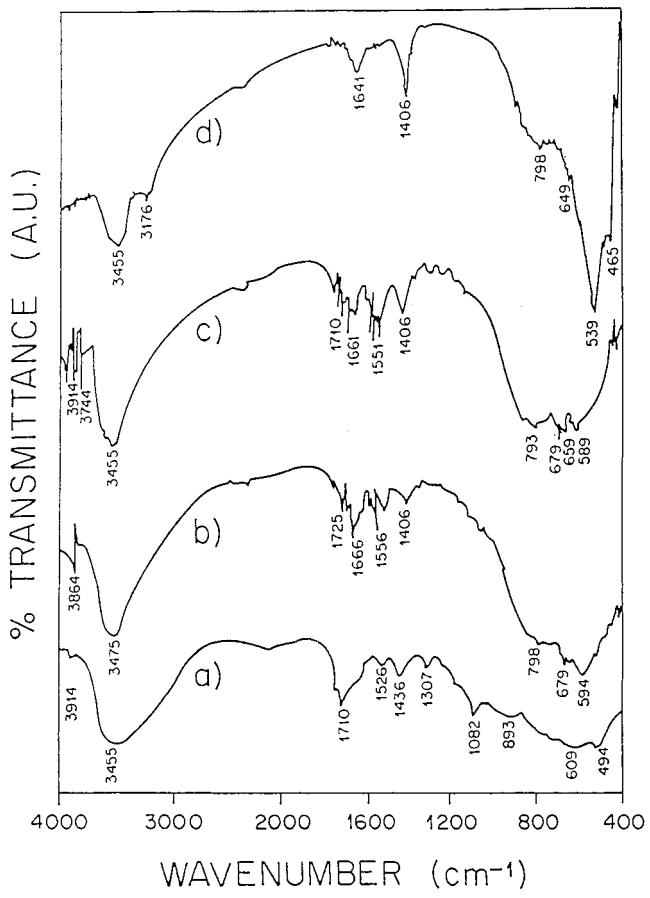

Figure 2. FTIR spectra of sol−gel alumina samples annealed at different temperatures: (a) 70; (b) 400; (c) 600; (d) 800 °C.

TABLE 1: Atomic Fractional Coordinates of γ-AlO(OH)[a]

atom	site	*x*	*y*	*z*
1Al	4c	0.166	0.250	0.0
1O	4c	0.213	0.250	0.0
2O	4c	0.433	0.250	0.0

[a] Unit cell is orthorhombic with space group *Cmcm*.

TABLE 2: Atomic Fractional Coordinates of γ-Al_2O_3[a]

atom	site	*x*	*y*	*z*
1Al	8a	0.125	0.125	0.125
2Al	16d	0.500	0.500	0.500
2O	32e	0.746	0.746	0.746

[a] Unit cell is cubic with space group *Fd*3*m*.

TABLE 3: Atomic Fractional Coordinates of θ-Al_2O_3[a]

atom	site	*x*	*y*	*z*
1Al	4i	0.079	0.0	−0.2012
2Al	4i	0.343	0.0	−0.2800
1O	4i	0.172	0.0	0.1011
2O	4i	0.496	0.0	0.2553
3O	4i	0.828	0.0	0.4365

[a] Unit cell is monoclinic with space group *C*2/*m*.

found for γ*-boehmite: $a = 2.805$ Å, $b = 15.631$ Å, and $c = 3.673$ Å, which differ from the corresponding parameters for γ-boehmite: $a = 3.201$ Å, $b = 13.601$ Å, and $c = 3.701$ Å (Figure 4).

The refinement showed that the γ*-boehmite structure was very disordered with many oxygen defects; the γ-boehmite structure also had oxygen defects but in a smaller number. When samples were annealed at 200 and 400 °C, the γ*-boehmite

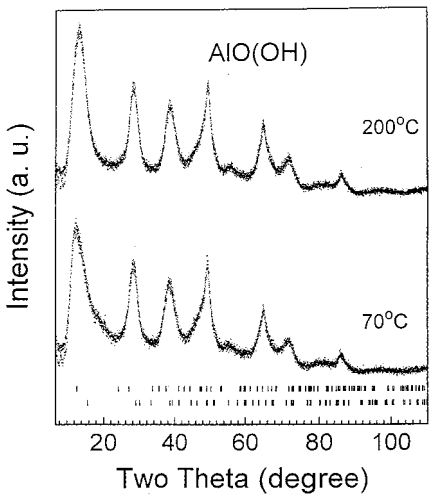

Figure 3. XRD patterns of sol−gel alumina samples annealed at 70 and 200 °C. Upper tick marks correspond to γ*-boehmite, the lower to γ-boehmite.

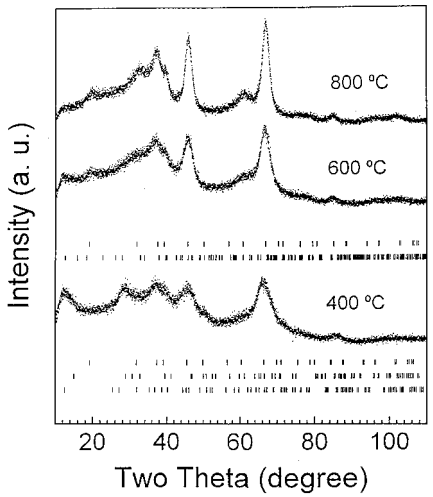

Figure 4. XRD patterns of sol−gel alumina samples annealed at 400, 600, and 800 °C. Below the diffraction pattern of the sample annealed at 600 °C, the upper tick marks correspond to γ-Al_2O_3, the lower to θ-Al_2O_3. Below the diffraction pattern of the sample annealed at 400 °C, upper tick marks correspond to γ-Al_2O_3, the middle tick marks to γ*-boehmite, and the lower to γ-boehmite.

TABLE 4. Phase Concentration (wt %)

T (°C)	γ*-AlO(OH)	γ-AlO(OH)	γ-Al_2O_3	θ-Al_2O_3
70	62.2	35.8		
200	87.8	12.2		
400	10.1	1.4	88.5	
600			71.9	28.2
800			64.0	36.0

concentration increased while that of γ-boehmite decreased, which indicates the transformation between the two phases (Table 4). This occurred because at higher sample calcining temperatures, the number of oxygen defects, via sample dehydroxylation, increased.

When the sample was annealed above 250 °C, the sample was dehydroxylated, destroying only boehmite hydroxyl layers but maintaining the boehmite oxygen layers unaffected. In this process, one-fourth of the total oxygen atoms were lost and the skeleton of the γ-Al_2O_3 crystalline structure was formed. During the transformation of boehmite into γ-Al_2O_3, the originally hexagonal oxygen arrangement, ABABAB..., was converted into the cubic arrangement, ABCABCABC....

TABLE 5: Average Crystallite Size (Å)

T (°C)	γ*-AlO(OH)	γ-AlO(OH)	γ-Al_2O_3	θ-Al_2O_3
70	31.5	42.1		
200	29.4	34.2		
400	23.7	34.2	55.4	
600			79.1	34.2
800			96.7	67.8

TABLE 6: Lattice Cell Parameters (Å)

T	γ*-AlO(OH)			γ-AlO(OH)			γ-Al_2O_3	θ-Al_2O_3		
(°C)	*a*	*b*	*c*	*a*	*b*	*c*	*a*	*a*	*b*	*c*
70	2.869	16.433	3.960	2.911	12.743	3.826				
200	2.859	16.059	3.939	2.882	12.727	3.787				
400	2.805	15.631	3.637	3.201	13.601	3.701	7.845			
600							7.849	13.691	2.283	5.525
800							7.858	13.691	2.823	5.525

Both the γ-boehmite and γ*-boehmite phases disappeared when the annealing temperature increased from 400 to 600 and 800 °C, yielding γ-Al_2O_3 and θ-Al_2O_3 (Table 4).

Tables 5 and 6 summarize the data obtained from the refinement of the crystalline structures. Annealing temperature strongly affected the lattice parameters and the average crystalline size, which ranged from 30 to 97 Å. These nanocrystalline structures gave rise to large specific surface areas and many nonsaturated bonds that make them attractive in catalysis.

Cationic and Anionic Defects in the Crystalline Structures. Since the defects in the alumina crystalline structure are related to its catalytic properties, they were analyzed and quantified in all phases. Structural defect concentrations were acquired by refining atom occupancy for each phase. All phases had defects; boehmite and θ-Al_2O_3 were oxygen deficient, but γ-Al_2O_3 was deficient in aluminum.

The oxygen deficiency in the crystalline structures of boehmite varied with the annealing temperature. For example, after annealing the sample at 200 °C, in the outside layer formed by OH groups, oxygen deficiency was about 30%. This corresponds to 1.8 vacancy sites per unit cell, like the one reported by Lipperns.[16]

Since in many cases γ-Al_2O_3 is selected as a catalyst or catalyst support,[35−38] the cationic deficiency in its crystalline structure has been carefully analyzed. γ-Al_2O_3 has a spinel crystalline structure. The prototype this structure, $A^{2+}B^{3+}{}_2O_4$, has 24 cations and 32 anions per unit cell. Eight A^{2+} cations are in the tetrahedral positions surrounded by four oxygen ions, and sixteen B^{3+} cations occupy the octahedral sites, coordinated to six oxygen ions. Because in γ-Al_2O_3 all aluminum ions are trivalent, in the fully dehydroxylated alumina, of the 24 sites in the lattice cell that can accept the cation, only 21.333 of them are occupied. In this case, the structure has 2.667 cationic defects per unit cell.[18]

The refinement of the γ-Al_2O_3 crystalline structure showed that the number of aluminum defects was higher than 2.667, the ideal number of defects for a fully dehydroxylated alumina. This is an indication that the sample was not totally dehydroxylated and some hydroxyls from boehmite persisted in the alumina structure. To preserve electron neutrality, some cationic defects must be created in the structure. The number of the cation defects must be equal to the number of OH ions in the structure.

Our results complemented Soled's study.[25] He assumes that hydroxyls are only on the crystal surface, but we found that they are also present in the bulk, as they are in nanocrystalline MgO,[39] TiO_2[40] and ZrO_2.[41] On the basis of electrical neutrality, he found that the number of vacancies is equal to the number of hydroxyls; from the refinement, we can obtain the number of vacancies but not the number of hydroxyls. Soled could not identify if the vacancies come from tetrahedral or octahedral sites; this, however, was obtained from the Rietveld refinement (Table 7).

TABLE 7: Aluminum Atom Occupancy and Defect Concentration in γ-Al_2O_3 Phase

	aluminum occupancy		number of defect sites		
T (°C)	tetrahedral	octahedral	N_1[a]	N_2[b]	N_t[c]
400	0.026	0.062	2.9	4.1	7.0
600	0.033	0.070	1.7	2.9	4.6
800	0.040	0.071	0.3	2.5	2.8

[a] N_1: number of aluminum vacancies per unit cell in tetrahedral position. [b] N_2: number of aluminum vacancies per unit cell in octahedral position. [c] N_t: total number of aluminum vacancies per unit cell.

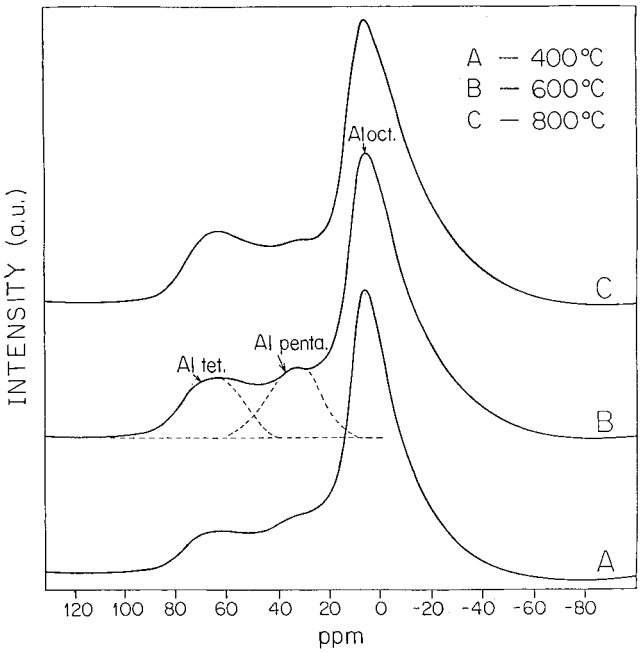

Figure 5. NMR-MAS spectra of alumina annealed at different temperatures.

We also observed that the concentration of the cationic defects in the octahedral positions was higher than that in the tetrahedral one (Table 7). When samples were annealed at 400 °C, 2.9 cation defects per unit cell appeared in the tetrahedral position and 4.1 in the octahedral one. When the annealing temperature increased from 400 to 600 and 800 °C, the total number of cationic defects per unit cell decreased from 7.0 to 4.6 and 2.8, respectively.

Aluminum Local Environment. When samples were annealed at 400 °C (Figure 5), their NMR spectra had three peaks: one centered at 5.6 ppm, another at 33.1 ppm, and one at 61.5 ppm. They correspond to the different local electron densities at the aluminum nucleus produced by the neighboring atoms. The peak at 5.6 ppm is typical of aluminum in oxygen octahedra, and the one located at 61.5 ppm is assigned to aluminum in oxygen tetrahedra.[43−45] The peak at 33.1 ppm corresponds to an aluminum nucleus surrounded by atoms that produce an electron density larger than that produced by an oxygen tetrahedra but smaller than the one produced by an oxygen octahedra.

In the literature, it is reported that the chemical shift at 33.1 ppm is produced by five oxygen atoms surrounding an aluminum nucleus.[42−44]

Since in our samples, some oxygen defects were found in the octahedral position of the θ-Al_2O_3 crystalline structure, we propose an alternative model for explaining this chemical shift. The driving force for creating oxygen defects, as suggested by T. Wood et al., seems to relate to the movement of aluminum ions from octahedral to tetrahedral sites.[45] Therefore, the electron density at the aluminum nucleus adjacent to an oxygen defect is lower than that produced by six oxygen neighbors but higher than that produced by the oxygen tetrahedra ambience. This would produce a chemical shift between 5 and 60 ppm.

In the sol−gel alumina samples used in the present work, however, hydroxyl groups were also present (Figure 2); these hydroxyls replace some of the oxygen atoms surrounding the aluminum atom in an octahedral symmetry, generating a lower electron density at the aluminum nucleus. Therefore, the observed chemical shift at 33.1 ppm could correspond to the unsaturated aluminum ion in an octahedral position (pentacoordinated aluminum ion) or to aluminum ions in octahedral symmetry surrounded by hydroxyls and oxygen ions as neighbors.

The NMR spectra of the samples annealed at 600 and 800 °C also had three peaks at 5.4, 35.3, and 65.3 ppm (Figure 4), which can be assigned to 4, 5, and 6-fold coordinated aluminum ions, respectively. The relative abundance of the different coordinated aluminum ions is a function of the thermal treatment.

Conclusions

The sol−gel γ-Al_2O_3 phase had aluminum vacancies produced by the incorporation of hydroxyl groups in its crystalline structure. These vacancies mainly corresponded to aluminum sites with octahedral symmetry; their concentration decreased when the sample annealing temperature increased.

In the γ-Al_2O_3 structure, at the nucleus of the aluminum atoms in the neighborhood of the hydroxyl groups, the electron density was smaller than that produced by oxygen octahedra, but larger than that produced by oxygen tetrahedra. This gave rise to a chemical shift in the NMR spectrum between the chemical shift produced for aluminum atoms in oxygen octahedra and the chemical shift produced for aluminum atoms in oxygen tetrahedra ambiance.

On the other hand, as a result of the existence of oxygen defects in the structure of θ-Al_2O_3 and boehmite, the observed chemical shift at 33.1 ppm was associated with unsaturated aluminum ions adjacent to oxygen defects in octahedral symmetry.

Since γ-Al_2O_3 and θ-Al_2O_3 were the main phases when samples were calcined at 400 and 800 °C, the OH groups and the cationic and anionic defects in the structures certainly will play an important role in their catalytic properties.

Acknowledgment. J. A. Wang would like to acknowledge the financial support from the CONACyT (Mexico) for his postdoctoral study at the Institute of Physics, of The National University of Mexico (UNAM). We also thank Mr. Edilberto Hernández for his kindly help in the XRD measurements.

References and Notes

(1) Yoldas, B. E. *J. Am. Chem. Soc.* **1982**, *65*, 387.
(2) Yoldas, B. E. Transparent Activated Nanoparticle Alumina and Method of Preparing Sample U.S. Patent 3, 941, 719, 1976.
(3) López, T.; Gómez, R. In *Sol−gel Optics* Klein, L. C., Ed.; Kluwer Academic Publishers: Boston, 1994; 345.
(4) Peri, J. B. *J. Phys. Chem.* **1965**, *69*, 211.
(5) Peri, J. B. *J. Phys. Chem.* **1965**, *69*, 231.
(6) Peri, J. B. *J. Phys. Chem.* **1966**, *70*, 3168.
(7) Imelik, B.; Mathieu, M. V.; Prette, M.; Teichner, S. J. *J. Chim. Phys. Fr.* **1954**, *51*, 651.
(8) Knozinger, H.; Ratnasamy, P. *Catal. Rev.—Sci. Eng.* **1978**, *7*, 31.
(9) Liu, P.; Skogsmo, J. *Acta Cryst. B* **1991**, *47*, 425.
(10) Vuorinen, S.; Skogsmo, J. In *Proceedings of the first International Conference on Surface Modification Techniques*, 1998; p 143.
(11) Krischner, H. *Ber. Dtsch. Keram. Ges.* **1966**, *43*, 479.
(12) Liu. P.; Skogamo, J. *Acta Cryst. B* **1991**, *47*, 425.
(13) Krischner, H. *Ber. Dtsch. Keram. Ges.* **1966**, *43*, 473.
(14) Kou, K. H.; Ye, H. Q.; Wu, Y. K. *Electron Diffraction Pattern with its Applications of Crystallography*; Science Press: Beijing, 1983 p 241.
(15) Okumiya, M.; Yamaguchi, G.; Yamada, O.; Ono, S. *Bull. Chem. Soc. Jpn.* **1971**, **44**, 418.
(16) Lippens, B. C.; Boer, J. H. *Acta Cryst.* **1964**, *17*, 1312.
(17) López, T.; Gómez, R.; Mendez-Vivar, J.; Campero, A. *Latin American Appl. Res.* **1990**, *20*, 167.
(18) Ervin, B. G. *Acta Crystallogr.* **1952**, *5*, 103.
(19) Tanabe, K. *Solid Acid and Bases*; Academic Press: New York, 1970.
(20) Tanabe, K.; Misono, M.; Ono, Y.; Hattori, H. *New Solid Acid and Bases*; Kodansha: Tokyo, 1989.
(21) Neyman, K. M.; Nasluzov, V. A. *Catal. Lett.* **1996**, *40*, 183.
(22) Zecchina, A.; Platero, E. E.; Arean, C. O. *J. Catal.* **1987**, *107*, 244.
(23) Kustov, L. M.; Kazansky, V. B. *J. Phys. Chem.* **1987**, *91*, 5247.
(24) Guillaume, D.; Gautier, S. *Catal. Lett.* ***1996***, *43*, 213.
(25) Soled, S. *J. Catal.* **1983**, *81*, 252.
(26) Young, R. A., Ed. *The Rietveld Method*; IUCr Monographs on Crystallography 5; Oxford University Press: New York, 1993.
(27) Skogsmo, J.; Liu, P. In *Proceedings of the Fifth European Conference on CVD*; Carlsson, J. O., Lindstron, J., Ed.; Uppsala University: Sweden, 1985; p 364.
(28) López, T.; Gómez, R.; Wang, J. A.; Novaro, O.; Bokhimi, Navarrete, J.; Llanos, M.; López-Salinas, E. *Mater. Lett.* **1997**, *32*, 325.
(29) López, T.; Romero, A.; Chavela, A.; Razo, L.; Gómez, R. *React. Kinet. Catal. Lett.* **1991**, *43*, 307.
(30) Yoldas, B. E. *J. Appl. Chem. Biotechnol.* **1973**, *23*, 803.
(31) Brinker, C. J.; Scherer, G. W. *Sol−gel Science*; Academic Press: New York, 1990.
(32) Young, R. A.; Von Dreele, R. "Rietveld Method Short Course", Continuing Education, Georgia Institute of Technology, April, 1993.
(33) Schneider, M. EDV-Vertrieb, Starnbergweg 18, D-8134 Pl̈cking, Germany. Personal communication, 1992.
(34) Wyckoff, R. W. G. *Crystal Structures*, reprint edition; Interscience Publisher: New York, 1982; Vol. 1, 294.
(35) Reichertz, P. P.; Yost, W. J. *J. Chem. Phys.* **1946**, *14* (8), 495.
(36) Gates, B. C.; Katzer, J. R.; Schuit, G. C. A. *Chemistry of Catalytic Processes*; McGraw-Hill: New York, 1979.
(37) Bond, C. G. *J. Catal.* **1997**, *166*, 192.
(38) Burch, R. *Catal. Lett.* **1997**, *43*, 19.
(39) Bokhimi, X.; Morales, A.; López, T.; Gómez, R. *J. Solid State Chem.* **1995**, *115*, 411.
(40) Bokhimi, A.; Morales, A.; Novaro, O.; López, T.; Sánchez, E.; Gómez, R. *J. Mater. Res.* **1995**, *10*, 2788.
(41) Bokhimi, X.; Morales, A.; Novaro, O.; Portilla, M.; López, T.; Tzompantzi, F.; Gómez, R. *J. Solid State Chem.* **1997**, *135*, 28.
(42) Chen, F. R.; Davis, J. G.; Fripiat, J. J. *J. Catal.* **1992**, *133*, 263.
(43) Dupree, R.; Farnan, I.; Forty, A. J.; El-Mashri, S.; Bottyan, L. *J. Phys. Colloq.* **1985**, *46*, 113.
(44) Pozarnsky, G. A.; McCormick, A. V. *J. Non-Cryst. Solid* **1995**, *190*, 212.
(45) Wood, T. E.; Siedle, A. R.; ill, J. R.; Skarjune, R. P.; Goodbrake, C. J. *Mater. Res. Soc. Symp. Proc.* **1990**, *180*, 97.